

2017

# The SWI/SNF protein PBRM1 restrains VHL-loss-driven clear cell renal cell carcinoma

James J. Hsieh

*Washington University School of Medicine in St. Louis*

et al

Follow this and additional works at: [https://digitalcommons.wustl.edu/open\\_access\\_pubs](https://digitalcommons.wustl.edu/open_access_pubs)

---

## Recommended Citation

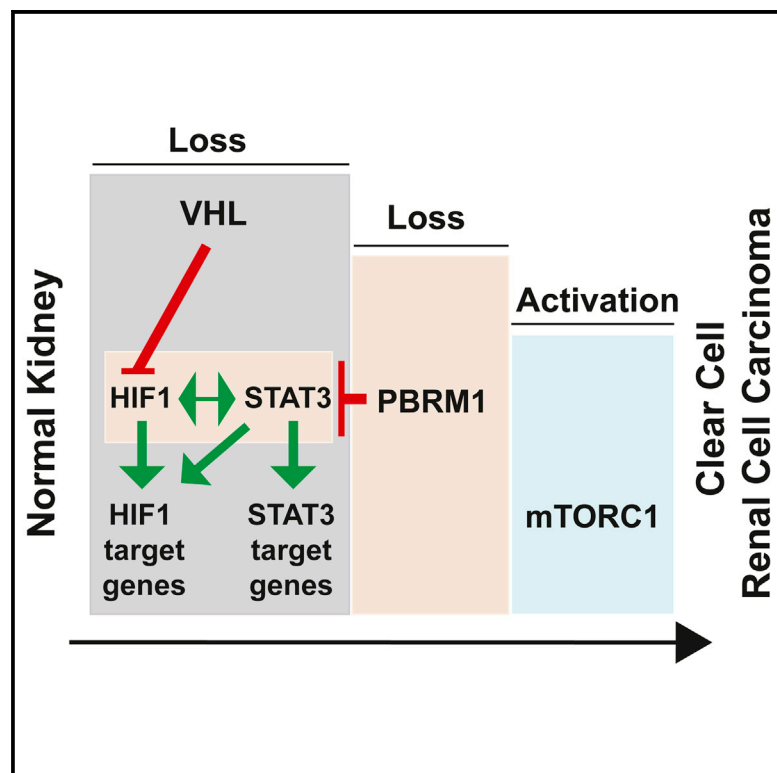
Hsieh, James J. and et al, "The SWI/SNF protein PBRM1 restrains VHL-loss-driven clear cell renal cell carcinoma." *Cell Reports*.18,12. 2893-2906. (2017).

[https://digitalcommons.wustl.edu/open\\_access\\_pubs/5756](https://digitalcommons.wustl.edu/open_access_pubs/5756)

This Open Access Publication is brought to you for free and open access by Digital Commons@Becker. It has been accepted for inclusion in Open Access Publications by an authorized administrator of Digital Commons@Becker. For more information, please contact [engeszer@wustl.edu](mailto:engeszer@wustl.edu).

# The SWI/SNF Protein PBRM1 Restrains VHL-Loss-Driven Clear Cell Renal Cell Carcinoma

## Graphical Abstract



## Authors

Amrita M. Nargund, Can G. Pham, Yiyu Dong, ..., Zhong Wang, Emily H. Cheng, James J. Hsieh

## Correspondence

cheng1@mskcc.org (E.H.C.), jhsieh@wustl.edu (J.J.H.)

## In Brief

Nargund et al. present a three-step process in the pathogenesis of mouse and human clear cell kidney cancer. After the loss of VHL, the loss of SWI/SNF tumor suppressor protein PBRM1/BAF180 further activates HIF1/STAT3 signaling in mouse kidney and positions mTORC1 activation as the preferred third driver event.

## Highlights

- PBRM1 is a bona fide tumor suppressor in the pathogenesis of ccRCC
- PBRM1 prevents self-perpetuating amplification of HIF1/STAT3 signaling in *Vhl*<sup>-/-</sup> cell
- Loss of *Vhl* and *Pbrm1* in mouse kidney results in multifocal, transplantable ccRCC
- In ccRCC, mTORC1 activation is the third driver event after loss of *VHL* and *PBRM1*

## Accession Numbers

GSE83688  
GSE83597



# The SWI/SNF Protein PBRM1 Restrains VHL-Loss-Driven Clear Cell Renal Cell Carcinoma

Amrita M. Nargund,<sup>1,14</sup> Can G. Pham,<sup>1,14</sup> Yiyu Dong,<sup>1,14</sup> Patricia I. Wang,<sup>1</sup> Hatice U. Osmangeyoglu,<sup>2</sup> Yuchen Xie,<sup>1,3</sup> Omer Aras,<sup>4</sup> Song Han,<sup>1</sup> Toshinao Oyama,<sup>1</sup> Shugaku Takeda,<sup>1</sup> Chelsea E. Ray,<sup>1</sup> Zhenghong Dong,<sup>1</sup> Mathieu Berge,<sup>1</sup> A. Ari Hakimi,<sup>5</sup> Sebastien Monette,<sup>6</sup> Carl L. Lekaye,<sup>7</sup> Jason A. Koutcher,<sup>8</sup> Christina S. Leslie,<sup>2</sup> Chad J. Creighton,<sup>11</sup> Nils Weinhold,<sup>9</sup> William Lee,<sup>9</sup> Satish K. Tickoo,<sup>10</sup> Zhong Wang,<sup>12</sup> Emily H. Cheng,<sup>1,10,\*</sup> and James J. Hsieh<sup>13,15,\*</sup>

<sup>1</sup>Human Oncology and Pathogenesis Program

<sup>2</sup>Department of Computational Biology

<sup>3</sup>Department of Radiology

<sup>4</sup>Gerstner Sloan Kettering School of Biomedical Sciences

<sup>5</sup>Department of Urology

<sup>6</sup>Laboratory of Comparative Pathology

<sup>7</sup>Department of Medical Physics

<sup>8</sup>Department of Medicine

<sup>9</sup>Department of Radiation Oncology

<sup>10</sup>Department of Pathology

Memorial Sloan Kettering Cancer Center, New York, NY 10065, USA

<sup>11</sup>Human Genome Sequencing Center, Baylor College of Medicine, Houston, TX 77030, USA

<sup>12</sup>Department of Cardiac Surgery, Cardiovascular Research Center, University of Michigan, Ann Arbor, MI 48109, USA

<sup>13</sup>Molecular Oncology, Department of Medicine, Siteman Cancer Center, Washington University, St. Louis, MO 63110, USA

<sup>14</sup>Co-first author

<sup>15</sup>Lead Contact

\*Correspondence: [chenge1@mskcc.org](mailto:chenge1@mskcc.org) (E.H.C.), [jhsieh@wustl.edu](mailto:jhsieh@wustl.edu) (J.J.H.)

<http://dx.doi.org/10.1016/j.celrep.2017.02.074>

## SUMMARY

***PBRM1* is the second most commonly mutated gene after *VHL* in clear cell renal cell carcinoma (ccRCC). However, the biological consequences of *PBRM1* mutations for kidney tumorigenesis are unknown. Here, we find that kidney-specific deletion of *Vhl* and *Pbrm1*, but not either gene alone, results in bilateral, multifocal, transplantable clear cell kidney cancers. *PBRM1* loss amplified the transcriptional outputs of HIF1 and STAT3 incurred by *Vhl* deficiency. Analysis of mouse and human ccRCC revealed convergence on mTOR activation, representing the third driver event after genetic inactivation of *VHL* and *PBRM1*. Our study reports a physiological preclinical ccRCC mouse model that recapitulates somatic mutations in human ccRCC and provides mechanistic and therapeutic insights into *PBRM1* mutated subtypes of human ccRCC.**

## INTRODUCTION

The estimated new kidney cancer cases diagnosed in the world and the United States every year are ~300,000 and ~63,000, respectively (Fitzmaurice et al., 2015; Siegel et al., 2016). Clear cell renal cell carcinoma (ccRCC) is the most common subtype (75%) (Hsieh et al., 2017b) and is lethal when metastasized

(Rini et al., 2009). The *Von Hippel-Lindau* (*VHL*) tumor suppressor gene is the most frequently mutated gene in ccRCC (Gnarra et al., 1994; Linehan et al., 1995) and its complete loss constitutes an early, truncal oncogenic driver event. *VHL* is the substrate recognition of an E3 ligase that labels hypoxia-inducible factor (HIF) 1 $\alpha$  and 2 $\alpha$  with ubiquitin for degradation (Kaelin, 2007; Majmundar et al., 2010; Masson and Ratcliffe, 2014; Semenza, 2013). Thus, human ccRCC is highly vascular due to uncontrolled activation of HIF $\alpha$  targets that regulate angiogenesis. Thereby, anti-vascular endothelial growth factor (VEGF)/vascular endothelial growth factor receptor (VEGFR) agents are effective, first-line treatment for metastatic ccRCC (mRCC) (Rini et al., 2009; Voss et al., 2013).

*VHL* inactivation was the only known oncogenic driver in ccRCC (Gnarra et al., 1994) until recent large-scale cancer genomic projects uncovered prevalent mutations including *PBRM1*/*BAF180* (29%–41%), *SETD2* (8%–12%), *BAP1* (6%–10%), and *KDM5C* (4%–7%) (Cancer Genome Atlas Research Network, 2013; Hakimi et al., 2013a; Peña-Llopis et al., 2012; Sato et al., 2013; Varela et al., 2011). Remarkably, these genes encode chromatin and epigenetic regulatory proteins, and most mutations are predicted to result in functional loss, favoring their roles as tumor suppressors (Hakimi et al., 2013b). *PBRM1*, the second most commonly mutated gene in all stages of ccRCC (Hsieh et al., 2017a), encodes BRG1-associated factor (BAF) 180, the defining subunit of the ~2 million dalton (MDa) polybromo BAF (PBAF) SWI/SNF complex (Varela et al., 2011). The SWI/SNF chromatin remodeling complexes are macromolecular machineries, which utilize ATP to mobilize



nucleosome and thereby modulate chromatin structure (Biegel et al., 2014; Clapier and Cairns, 2009). They regulate critical cellular processes, including cell-cycle, cell fate, cell death, metabolism, and DNA repair (Hargreaves and Crabtree, 2011). Interestingly, pan-cancer genomics have uncovered epigenetic regulators including SWI/SNF proteins as a major class of cancer genes (Dawson and Kouzarides, 2012). Mutations of individual SWI/SNF subunits have been detected in ~20% of human cancers and they displayed preferential enrichment of mutations among cancer types (Helming et al., 2014; Kadoch et al., 2013; Marquez et al., 2015). For example, *PBRM1* is most highly mutated in ccRCC, *SMARCB1* (*BAF47*) in pediatric rhabdoid tumors and *ARID1A* (*BAF250A*) in ovarian clear cell carcinoma (Biegel et al., 2014), implicating underlying tissue tropism for disarming specific tumor suppressor gene (TSG) during tumorigenesis (Wei and Hsieh, 2015).

The knowledge of *PBRM1* in mammalian biology is limited. Mice with straight knockout of *Pbrm1* resulted in embryonic lethality at embryonic day 11.5 due to heart defects (Huang et al., 2008; Wang et al., 2004), whereas mice with T lymphocyte-specific knockout of *Pbrm1* exhibited normal thymus and peripheral T cell development (Wurster et al., 2012). In vitro studies demonstrated that *PBRM1* activated p21 upon irradiation in breast cancer cell lines (Xia et al., 2008) and participated in p53-induced replicative senescence in fibroblasts (Burrows et al., 2010), and *PBRM1* knockdown enhanced proliferation and migration of kidney cancer cell lines (Varela et al., 2011). However, the in vivo tumor suppressor function of *PBRM1* has not been established, and how *PBRM1* loss-of-function promotes tumorigenesis remains unclear.

The long latency (>30 years) for *VHL* germline-mutated patients to develop ccRCC (Fisher et al., 2014; Kaelin, 2007) and the inability of *Vhl* deficiency to induce ccRCC in mice (Kapitsinou and Haase, 2008) suggest that additional genetic/epigenetic events are probably needed for the development of ccRCC (Wei and Hsieh, 2015). *PBRM1* loss-of-function is one of the most likely candidates given its high mutation frequency (~40%) in human ccRCC (Hsieh et al., 2017a). Here, we created kidney-specific deletion of *Pbrm1* and/or *Vhl* mice to study the tumor suppressor role of *PBRM1* and sought to establish a physiological mouse kidney cancer model that recapitulates human ccRCC.

## RESULTS

### Genetic Deletion of *Pbrm1* in Mouse Kidney Results in Hydronephrosis

As *Pbrm1* (*BAF180*) deletion in mice incurred embryonic lethality (Wang et al., 2004), we deleted the conditional *Pbrm1*<sup>F/F</sup> allele (Wurster et al., 2012) in the mouse kidney using a transgenic Cre recombinase line Ksp-Cre (Shao et al., 2002) that has been widely utilized to model kidney cancer in mice (Adam et al., 2011; Baba et al., 2008; Chen et al., 2008; Igarashi, 2004). The expression of Cre from the Ksp-Cre is driven by the kidney-specific *Cadherin 16* promoter, which begins expression at embryonic day 14.5 in epithelial cells of the developing kidney and genitourinary tract and continues to be expressed in tubular epithelial cells in adults. *Pbrm1*<sup>F/F</sup>Ksp-Cre mice were born at expected Mendelian ratio. To monitor if *Pbrm1* loss results in any

gross kidney abnormality, serial abdominal MRI was performed on a large cohort of mice. Obstructive hydronephrosis, enlarged kidneys containing fluid-filled renal pelvis, and non-neoplastic masses at the ureteropelvic junction or proximal ureter were detected in some *Pbrm1*<sup>F/F</sup>Ksp-Cre mice (Figures 1A and S1A). Among 53 *Pbrm1*<sup>F/F</sup>Ksp-Cre and 27 *Pbrm1*<sup>+/+</sup>Ksp-Cre (denoted as *WT* thereafter) mice examined, 18 (34%) *Pbrm1*<sup>F/F</sup>Ksp-Cre while 0 *WT* mice developed hydronephrosis (Figure 1B). Observed hydronephrosis exhibited a preponderance of female over male and left over right (Figures 1C and 1D) and could be detected by MRI as early as 6 months of age (Figure S1B). At necropsy, the volume of hydronephrotic *Pbrm1*<sup>F/F</sup>Ksp-Cre kidneys was at two to five times that of normal appearing kidneys (Figure 1E), whereas the creatinine of aged *Pbrm1*<sup>F/F</sup>Ksp-Cre and *WT* mice was comparable (Figure 1F).

### Genetic Deletion of *Vhl* and *Pbrm1* in Mouse Kidney Results in Polycystic Kidney Disease and Increased Mortality

As neither *Vhl* nor *Pbrm1* deletion alone caused kidney tumors, *Vhl*<sup>F/F</sup>*Pbrm1*<sup>F/F</sup>Ksp-Cre mice were generated to investigate the genetic interaction between *Vhl* and *Pbrm1* deficiency in kidney cancer pathogenesis. The survival of 325 mice (36 *WT*, 30 *Vhl*<sup>F/F</sup>Ksp-Cre, 129 *Pbrm1*<sup>F/F</sup>Ksp-Cre, and 130 *Vhl*<sup>F/F</sup>*Pbrm1*<sup>F/F</sup>Ksp-Cre) was monitored, which revealed a markedly increased mortality in *Vhl*<sup>F/F</sup>*Pbrm1*<sup>F/F</sup>Ksp-Cre mice and a moderately increased mortality in *Vhl*<sup>F/F</sup>Ksp-Cre mice (Figure 2A). Remarkably, abdominal MRI detected diffuse polycystic kidney disease (PKD) in 30% (17/56) of 6- to 9-month-old and in 67% (14/21) of 10- to 14-month-old *Vhl*<sup>F/F</sup>*Pbrm1*<sup>F/F</sup>Ksp-Cre mice, whereas only 1 of 14 aged *Vhl*<sup>F/F</sup>Ksp-Cre mice (12- to 16-month-old) developed PKD with a few scattered cysts (Figures 2B, 2C, and S2). To investigate cystic changes, we performed histological analysis on the kidneys of *Vhl*<sup>F/F</sup>*Pbrm1*<sup>F/F</sup>Ksp-Cre mice at different ages (3–13 months). Both tubular and glomerular cysts were present in young mice (Figure S3). Of note, scattered cystic anomalies of kidneys have been described in hereditary *VHL* patients and are implicated as pre-neoplastic lesions (Mandriota et al., 2002; Neumann and Zbar, 1997; Walther et al., 1995). Consistent with a prior report, mild hydronephrosis was also observed in *Vhl*<sup>F/F</sup>Ksp-Cre mice (Figure 2D) (Frew et al., 2008). Elevated serum creatinine was observed in the majority of aged *Vhl*<sup>F/F</sup>*Pbrm1*<sup>F/F</sup>Ksp-Cre mice (Figure 2E), which could be accountable for their early demise.

### *Vhl*<sup>F/F</sup>*Pbrm1*<sup>F/F</sup>Ksp-Cre Mice Develop Multifocal, Clear Cell Kidney Cancer

Serial MRI examination of kidney in *Vhl*<sup>F/F</sup>*Pbrm1*<sup>F/F</sup>Ksp-Cre mice recognized patterns of imaging changes from normal through progressive cystic abnormality to increased multifocal nodularity with decreased cystic appearance (Figures S2 and S3). Gross examination of 58 kidneys (29 mice, 8- to 17-month-old) at necropsy showed diffusely cystic changes in 58.33% (21/36) of *Vhl*<sup>F/F</sup>*Pbrm1*<sup>F/F</sup>Ksp-Cre kidneys and none in *Vhl*<sup>F/F</sup>Ksp-Cre (n = 8), *Pbrm1*<sup>F/F</sup>Ksp-Cre (n = 10), and *WT* (n = 4) kidneys (Table S1). Histologic examination revealed sheets of tumor cells interspersed within a highly vascularized stroma in 33.33% (12/36) *Vhl*<sup>F/F</sup>*Pbrm1*<sup>F/F</sup>Ksp-Cre kidneys, whereas no tumors were noted in 22 kidneys of the other genotypes (Table S1). Notably, all the

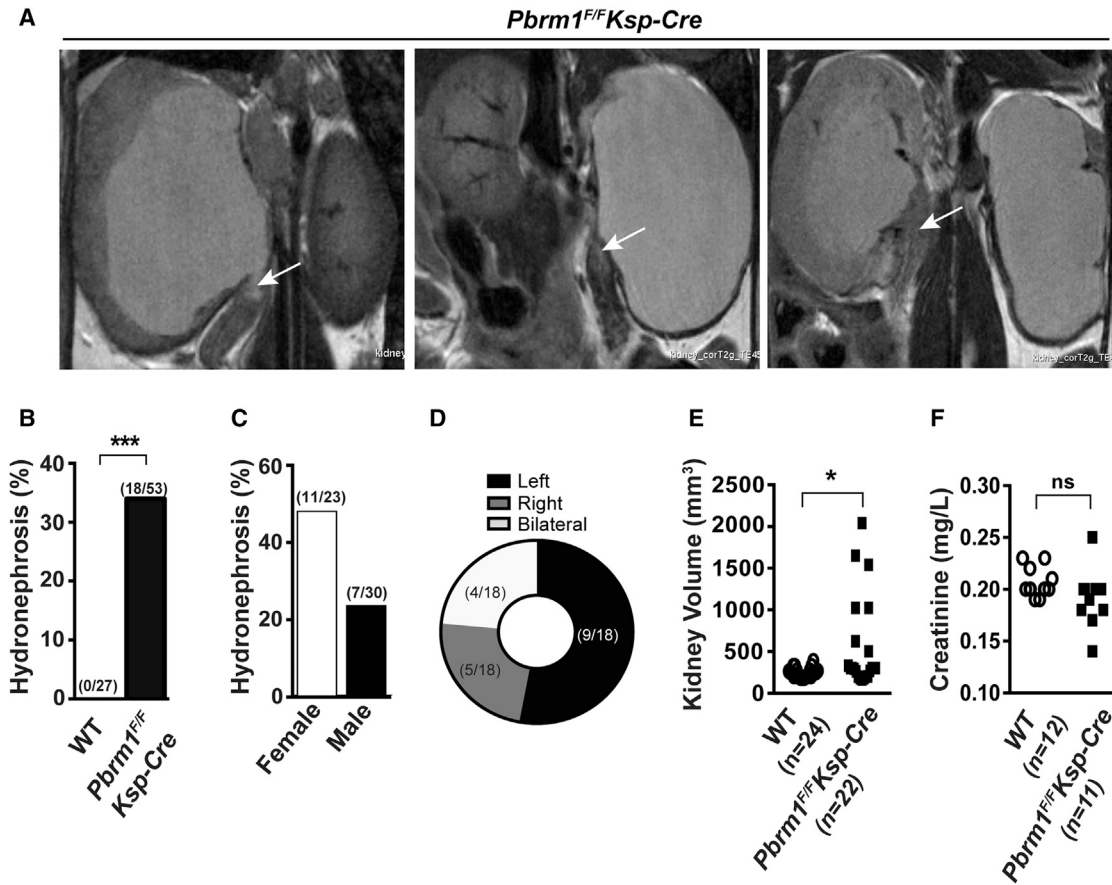


**Figure 1. *Pbrm1<sup>F/F</sup>Ksp-Cre* Mice Develop Obstructive Hydronephrosis**

(A) Representative MRI images of unilateral or bilateral severe hydronephrosis. The non-neoplastic mass at the proximal ureter is marked by arrow. (B) Incidence of hydronephrosis in WT and *Pbrm1<sup>F/F</sup>Ksp-Cre* mice. Cohorts of animals at 12 months of age on average were randomly selected for MRI scanning. \*\*\* $p < 0.001$  (Fischer's exact). (C) Incidence of hydronephrosis in the *Pbrm1<sup>F/F</sup>Ksp-Cre* mice based on gender. (D) Location distribution of hydronephrosis in *Pbrm1<sup>F/F</sup>Ksp-Cre* mouse kidneys. (E) Kidney volume in WT and *Pbrm1<sup>F/F</sup>Ksp-Cre* mice. \* $p < 0.05$  (Mann-Whitney). (F) Serum creatinine levels of mice in (E). ns, not statistically significant.

tumors were observed in *Vhl<sup>F/F</sup>Pbrm1<sup>F/F</sup>Ksp-Cre* mice after 10 months of age with a 50% tumor incidence (12/24). The tumor cells displayed central features of human ccRCC, including clear cytoplasm and positive membranous staining of carbonic anhydrase IX (CA-IX), a target of HIF1 (Mandriota et al., 2002; Semenza, 2013) (Figure 3A). Consistent with the known aberrant HIF1 activation in the absence of VHL, weak, sporadic CA-IX staining was detected in *Vhl<sup>F/F</sup>Ksp-Cre*, but not in *Pbrm1<sup>F/F</sup>Ksp-Cre* or WT kidneys (Figure 3A). To compare these mouse tumors with human RCCs, we performed gene expression profile analysis of these mouse tumors in comparison to human TCGA clear cell RCC (KIRC) and chromophobe RCC (KICH) kidney cancers and demonstrated that *Vhl<sup>F/F</sup>Pbrm1<sup>F/F</sup>Ksp-Cre* tumors resemble KIRC but not KICH (Figure 3B). Data suggest that human clear cell RCC arises from proximal tubule (Chen et al., 2016). Accordingly, we investigated the cell type origin of *Vhl<sup>F/F</sup>Pbrm1<sup>F/F</sup>Ksp-Cre* mouse tumors. Staining for lotus tetragonolobus lectin (LTL) that marks proximal convoluted tubule

and for Tamm-Horsfall protein (THP) that marks distal convoluted tubule was performed. Consistent with human ccRCC originating from proximal tubule, our *Vhl<sup>F/F</sup>Pbrm1<sup>F/F</sup>Ksp-Cre* mouse tumors were stained positive for LTL but not THP (Figure 3C). CD45 staining did not detect increased lymphocyte infiltrate of these *Vhl<sup>F/F</sup>Pbrm1<sup>F/F</sup>Ksp-Cre* tumors (Figure 3C). Consistent with human ccRCC reports, these tumors were positive for CD31 staining that marks endothelial cells (Figure 3C). We also performed Oil Red O staining of the fresh frozen section of these mouse tumors to evaluate lipid content in our the clear cell mouse tumors (Figure S4). Furthermore, the presence of high glycogen in these tumors was confirmed by PAS-D staining (Figure S4). Of note, our *Vhl<sup>F/F</sup>Pbrm1<sup>F/F</sup>Ksp-Cre* mouse tumors did not directly originate from cystic lesions (Figure S5A). Higher proliferation index (Ki-67 staining) was observed in these *Vhl* and *Pbrm1* doubly deficient clear cell kidney tumors whereas no alteration in cell death was detected by immunohistochemistry for cleaved caspase-3 and TUNEL assays (Figures S5B

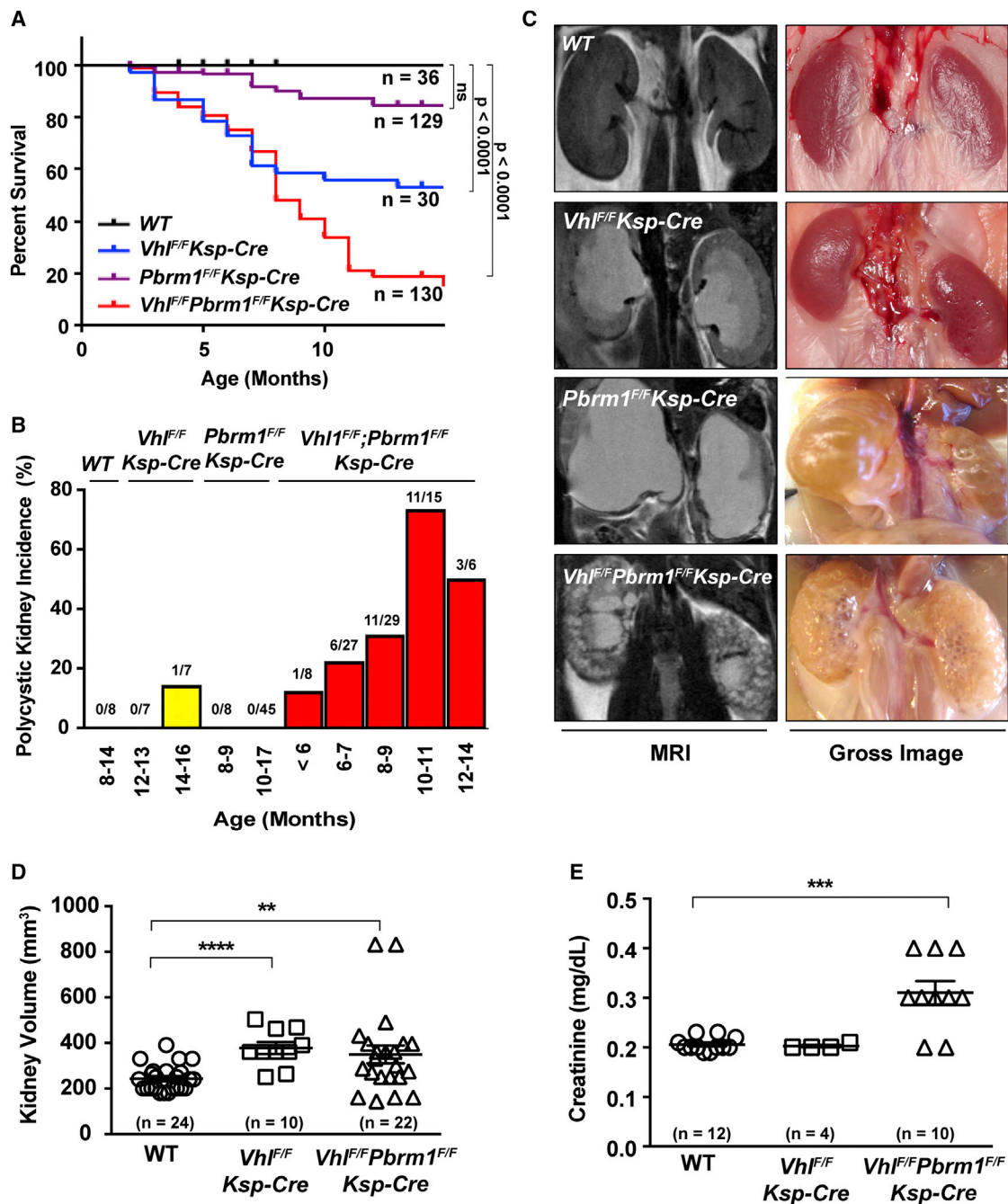


**Figure 2. *Vhl*<sup>F/F</sup>*Pbrm1*<sup>F/F</sup>*Ksp-Cre* Mice Develop Polycystic Kidney Disease and Exhibit Premature Mortality**

(A) Kaplan-Meier survival curve of WT, *Vhl*<sup>F/F</sup>*Ksp-Cre*, *Pbrm1*<sup>F/F</sup>*Ksp-Cre*, and *Vhl*<sup>F/F</sup>*Pbrm1*<sup>F/F</sup>*Ksp-Cre* mice.

(B) Incidence of polycystic kidney disease in WT, *Vhl*<sup>F/F</sup>*Ksp-Cre*, *Pbrm1*<sup>F/F</sup>*Ksp-Cre*, and *Vhl*<sup>F/F</sup>*Pbrm1*<sup>F/F</sup>*Ksp-Cre*. Age and number of animals in each group are specified.

(C) Representative MRI and gross images of kidneys of the indicated genotypes.

(D) Kidney volumes of WT, *Vhl*<sup>F/F</sup>*Ksp-Cre*, and *Vhl*<sup>F/F</sup>*Pbrm1*<sup>F/F</sup>*Ksp-Cre* mice. Numbers of kidneys measured in each group (n) are indicated. \*\*p = 0.0096; \*\*\*p < 0.0001 (Mann-Whitney).

(E) Serum creatinine levels in WT, *Vhl*<sup>F/F</sup>*Ksp-Cre*, and *Vhl*<sup>F/F</sup>*Pbrm1*<sup>F/F</sup>*Ksp-Cre* mice (the same as Figure 1D). \*\*\*p < 0.001 (Mann-Whitney).

and S5C). qPCR with reverse transcription (qRT-PCR) demonstrated greatly reduced *Vhl* and *Pbrm1* expression in *Vhl*<sup>F/F</sup>*Pbrm1*<sup>F/F</sup>*Ksp-Cre* kidney tumors (Figure S5D). Of note, we did

not detect local tumor invasion into adjacent tissues or distant metastasis to lungs, livers, bones, and lymph nodes in the examined tumor-bearing *Vhl*<sup>F/F</sup>*Pbrm1*<sup>F/F</sup>*Ksp-Cre* mice.

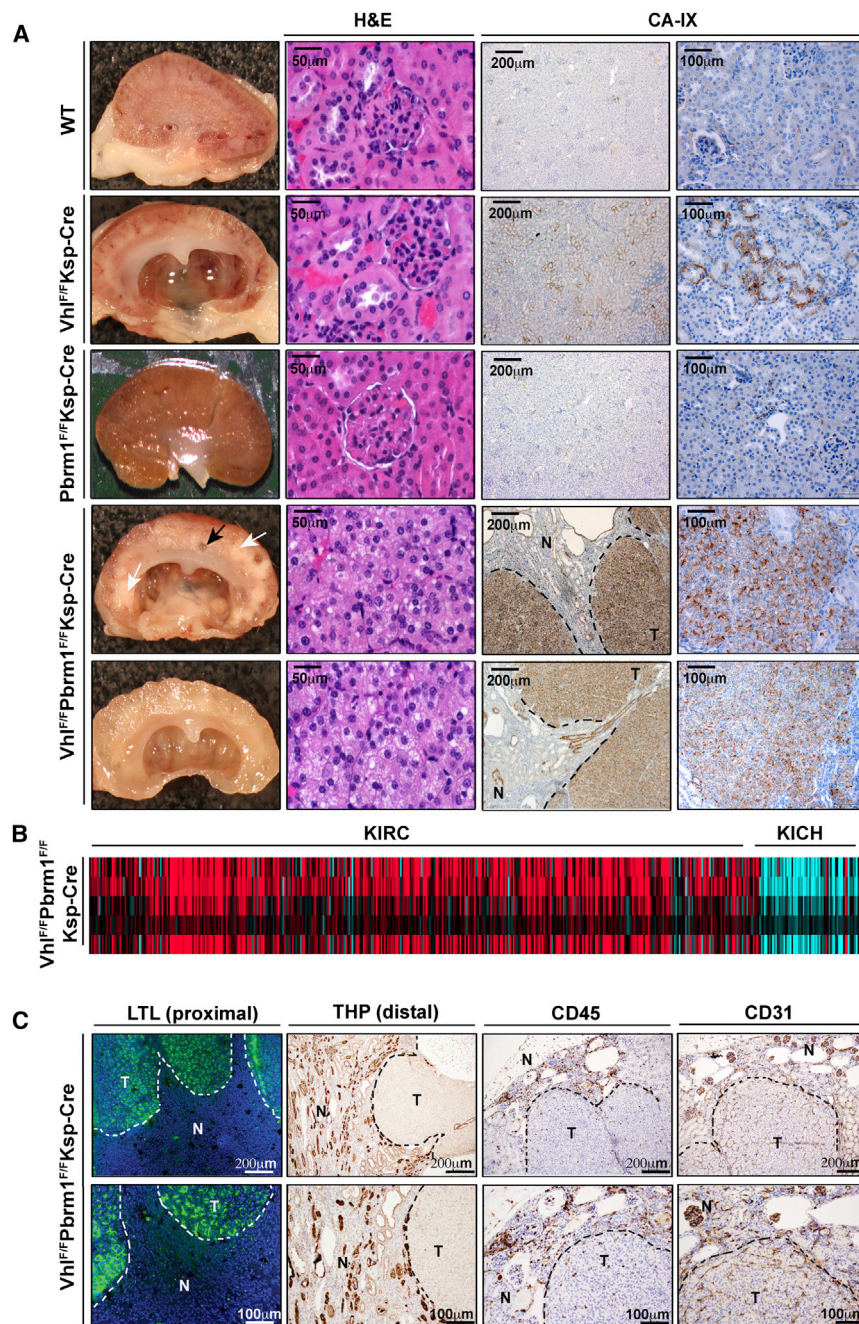


**Figure 3. *Vhl*<sup>F/F</sup>*Pbrm1*<sup>F/F</sup>*Ksp-Cre* Mice Develop Multifocal CA-IX Positive Clear Cell Kidney Cancers**

(A) Representative gross images (column 1), histopathological images (column 2), and immunohistochemistry of CA-IX (columns 3 and 4) of WT, *Vhl*<sup>F/F</sup>*Ksp-Cre*, *Pbrm1*<sup>F/F</sup>*Ksp-Cre*, and *Vhl*<sup>F/F</sup>*Pbrm1*<sup>F/F</sup>*Ksp-Cre* kidneys. Tumor and cyst are indicated by white and black arrows, respectively. T, tumor; N, adjacent normal. Scale bars are at 50  $\mu$ m, 100  $\mu$ m, or 200  $\mu$ m as indicated.

(B) Heatmap of inter-sample correlations (red, positive) between mRNA profiles of TCGA human RCC tumors (columns, TCGA KIRC and KICH data) and *Vhl*<sup>F/F</sup>*Pbrm1*<sup>F/F</sup>*Ksp-Cre* mouse kidney tumors (rows).

(C) Representative images of immunofluorescence of LTL (column 1) and immunohistochemistry of THP (column 2), CD45 (column 3), and CD31 (column 4) in *Vhl*<sup>F/F</sup>*Pbrm1*<sup>F/F</sup>*Ksp-Cre* tumors and adjacent non-tumor tissues.

Furthermore, tumors that developed in the transplanted NSG mouse could be further successfully propagated into a NSG mouse (Figure 4A). Together, these data demonstrated the malignant potential of *Vhl*<sup>F/F</sup>*Pbrm1*<sup>F/F</sup>*Ksp-Cre* mouse kidney tumors. Histology of these tumor allografts showed the same histological features, positive CA-IX staining as donor tumors, and genotypes (Figure 4). Importantly, this stepwise, morphological progression observed in *Vhl*<sup>F/F</sup>*Pbrm1*<sup>F/F</sup>*Ksp-Cre* kidneys from normal appearance through cystic changes (~6 months) to ccRCC formation (~10 months) offered an opportunity to temporally dissect the mechanisms by which PBRM1 loss cooperates with VHL loss to initiate the development of ccRCC.

**Gene Expression Profiling of WT, *Vhl*-Deficient, *Pbrm1*-Deficient, or *Vhl* and *Pbrm1* Doubly Deficient Mouse Renal Cortices Identifies Distinct Clusters**

To determine why double deficiency of *Vhl* and *Pbrm1*, but not single deficiency

***Vhl* and *Pbrm1* Doubly Deficient Clear Cell Kidney Tumors Are Transplantable**

To assess the tumor initiating capacity of the de novo *Vhl* and *Pbrm1* doubly deficient kidney tumors, we transplanted 12 tumor fragments from two *Vhl*<sup>F/F</sup>*Pbrm1*<sup>F/F</sup>*Ksp-Cre* kidneys into the sub-renal capsules of 12 kidneys of 6 immunocompromised *NOD/SCID/IL2R $\gamma$ <sup>null</sup>* (NSG) mice. All the recipient kidneys, except for the one animal that died prematurely of known cause, showed large visible kidney tumors upon dissection at 10–12 months after transplantation (Figure 4A). In two of the transplanted cases, we also observed tumor invasion into organs such as liver (Figure 4B).

of either gene, resulted in ccRCC, we performed gene expression profiling of RNA isolated from renal cortices of 12-week-old WT, *Vhl*<sup>F/F</sup>*Ksp-Cre*, *Pbrm1*<sup>F/F</sup>*Ksp-Cre*, and *Vhl*<sup>F/F</sup>*Pbrm1*<sup>F/F</sup>*Ksp-Cre* mice. Kidneys from 12-week-old mice were chosen to avoid potentially confounding transcriptional changes secondary to cystic anomalies that normally manifest after 6 months of age. Of note, none of the 12-week-old mouse kidneys displayed discernible macroscopic or microscopic cystic abnormalities at necropsy regardless of genotypes. Genes differentially expressed in at least one genotype were identified (Table S2A) and subjected to unsupervised hierarchical

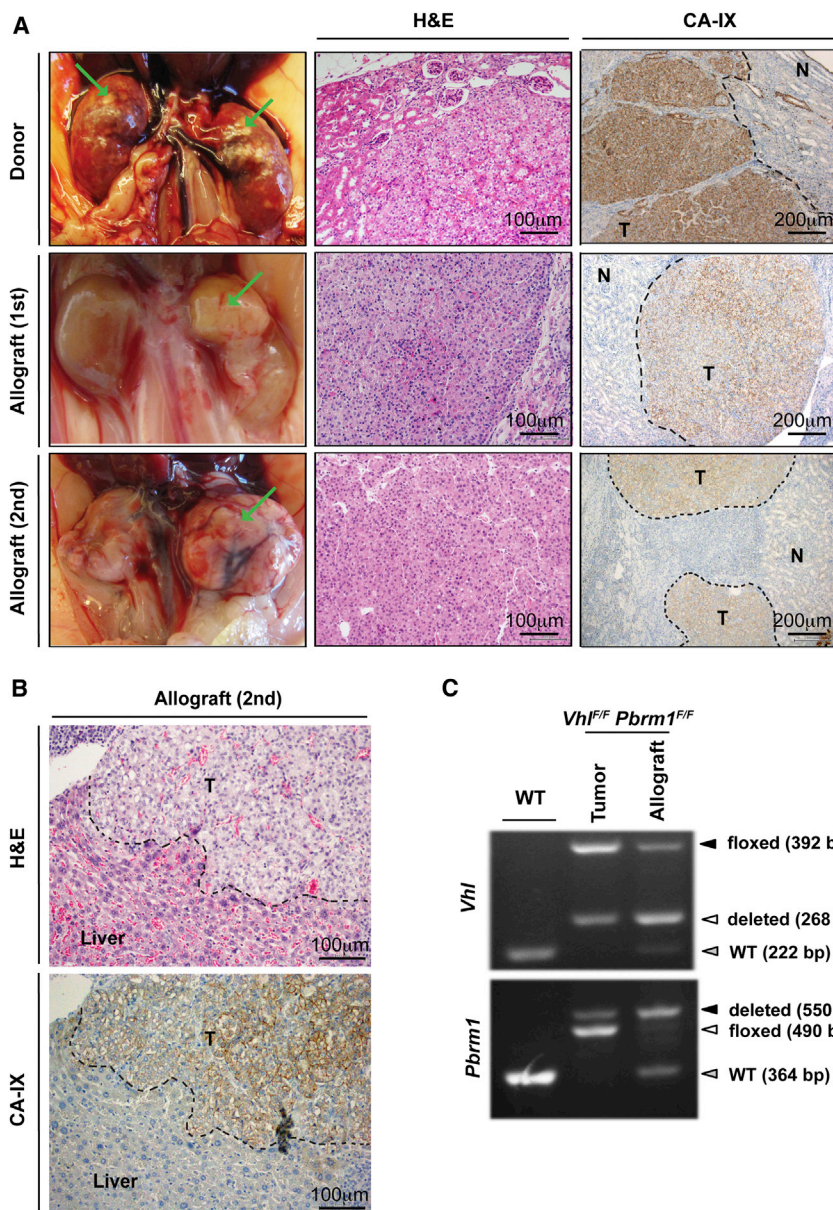


**Figure 4. *Vhl*<sup>F/F</sup>*Pbrm1*<sup>F/F</sup>*Ksp-Cre* Mice Tumors Are Transplantable and Invasive**

(A) Representative gross images (column 1), histopathological images (column 2), and immunohistochemistry of CA-IX (column 3) of donor *Vhl*<sup>F/F</sup>*Pbrm1*<sup>F/F</sup>*Ksp-Cre* kidney tumors (row 1), primary allograft kidney tumors (row 2), and secondary allograft kidney tumors (row 3).

(B) Representative histopathological image (top) and immunohistochemistry of CA-IX (bottom) of the transplanted invasive tumors.

(C) PCR genotyping of WT kidney and donor and allograft *Vhl*<sup>F/F</sup>*Pbrm1*<sup>F/F</sup>*Ksp-Cre* tumors.

### PBRM1 Loss Amplifies the Transcriptional Outputs of HIF1 and STAT3 Incurred by VHL Loss

HIF1 $\alpha$  is stabilized upon VHL loss and plays a central role in the pathogenesis of ccRCC. It was reported that HIF1 induces PKM2 to activate STAT3, which in turn induces HIF1 $\alpha$  expression (Demaria and Poli, 2012; Luo and Semenza, 2012). Furthermore, it is known that HIF1 and STAT3 cooperate to activate the expression of HIF1 targets including genes involved in angiogenesis (Jung et al., 2005). Consequently, the intricate interplay between HIF1 and STAT3 establishes a feed-forward amplification loop to maximize target gene expression. Our discovery that HIF1 and JAK-STAT pathway genes were enriched in *Vhl*-deficient renal cortices and further enriched in *Vhl* and *Pbrm1* doubly deficient renal cortices raises a hypothesis in which PBRM1 prevents the amplification of the HIF1 and STAT3 transcriptional outputs that are initiated upon VHL loss.

To test this, we identified HIF1 and STAT3 motifs from differentially expressed genes to determine the strength of regulation of the targets by individual transcription factor binding motifs

clustering analysis, which revealed three distinct clusters (Figure 5A). Cluster I showed enrichment of genes that were upregulated in *Vhl*-deficient renal cortices and further upregulated in *Vhl* and *Pbrm1* doubly deficient renal cortices. In contrast, cluster III showed enrichment of genes that were downregulated in *Vhl* and *Pbrm1* doubly deficient renal cortices. Each cluster was then analyzed and visualized using ClueGO (Bindea et al., 2009) to interrogate functionally grouped gene ontology and pathway networks (Figure 5B; Table S2B). Pathways over-represented that are highly pertinent to known ccRCC pathogenesis were HIF1 and JAK-STAT pathway genes in cluster I and oxidative phosphorylation (OXPHOS) genes in cluster III (Figure 5B), whereas no pathway was significantly enriched in cluster II.

(TFBMs). RNA expression data were analyzed using Integrated System for Motif Activity Response Analysis (ISMARA) (Balwiercz et al., 2014), which produced an output denoting the inferred activity of HIF1 and STAT3 motifs in every sample. An increase in the HIF1 ( $p = 0.08$ ) and STAT3 ( $p = 0.017$ ) motif activities was detected when comparing *Vhl*<sup>F/F</sup>*Ksp-Cre* to WT kidneys, and a marked increase in both HIF1 ( $p = 0.00076$ ) and STAT3 ( $p = 0.00018$ ) outputs was identified when comparing *Vhl*<sup>F/F</sup>*Pbrm1*<sup>F/F</sup>*Ksp-Cre* to WT kidneys. In contrast, no changes in HIF1 ( $p = 0.49$ ) or STAT3 ( $p = 0.98$ ) motif activity were observed when comparing *Pbrm1*<sup>F/F</sup>*Ksp-Cre* to WT kidneys. Remarkably, the effects of *Pbrm1* deletion on HIF1 and STAT3 targets manifested only under the premise of *Vhl* loss, resulting in a further increase of the HIF1 ( $p = 0.035$ ) and STAT3 ( $p = 0.0022$ ) motif



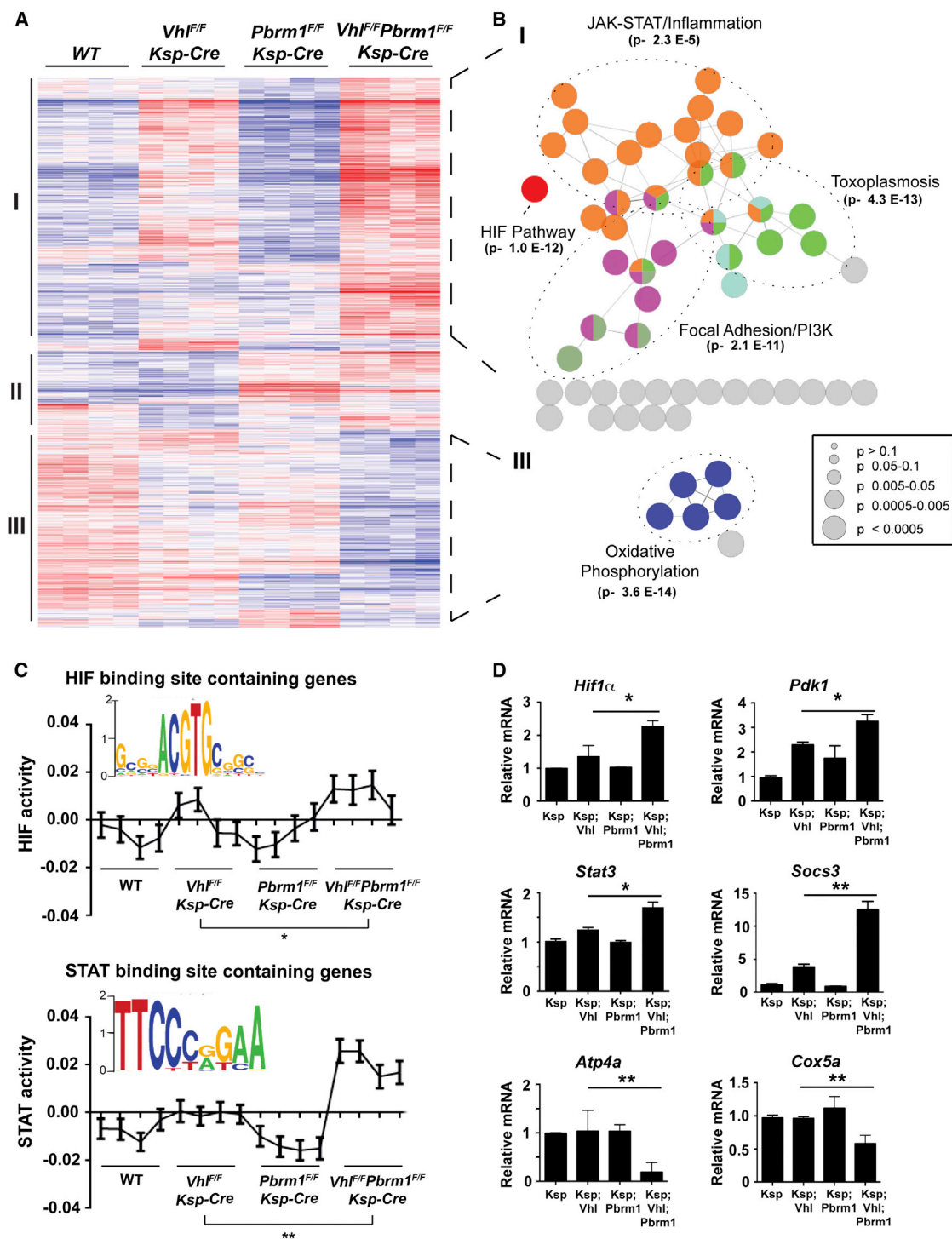


**Figure 5. PBRM1 Loss Amplifies the Transcriptional Outputs of HIF1 and STAT3 Incurred by VHL Loss**

(A) Heatmap of genes with significantly different expression in the renal cortices of WT, *Vhl<sup>F/F</sup>Ksp-Cre*, *Pbrm1<sup>F/F</sup>Ksp-Cre*, and *Vhl<sup>F/F</sup>Pbrm1<sup>F/F</sup>Ksp-Cre* mice at 12 weeks of age. Unsupervised hierarchical agglomerative clustering identified three distinct clusters using Pearson correlation and average linkage as similarity measures for pairs of genes and pairs of inchoate clusters, respectively.

(B) Clusters I and III were tested for pathway enrichment and presented using ClueGO.

(C) Inferred HIF and STAT motif activities across the indicated genotypes. \*p = 0.035; \*\*p = 0.0022 (one-sided t test).

(D) The mRNA levels of the indicated genes from the indicated genotypes were assessed by qRT-PCR. Data were normalized against GAPDH (mean ± SD, n = 3 independent experiments). \*p < 0.05; \*\*p < 0.005 (Student's t test).

activities when comparing *Vhl*<sup>F/F</sup>*Pbrm1*<sup>F/F</sup>*Ksp-Cre* to *Vhl*<sup>F/F</sup>*Ksp-Cre* kidneys (Figure 5C). To further validate these findings, we performed qRT-PCR analyses on *Hif1a*, *Stat3*, and representative HIF1 target genes (*Pdk1* and *Egln3*) as well as STAT3 target genes (*Socs3*, *Il4r*, and *Il6r*) (Figures 5D and S6A–S6D), which demonstrated consistent results among different gene expression assays. Of note, we did not see any transcriptional upregulation of HIF2 $\alpha$ . In summary, our data suggest that PBRM1, a SWI/SNF complex protein, could function like a transcriptional resistor to prevent uncontrolled self-perpetuating amplification of the HIF1 and STAT3 transcriptional outputs incurred by *Vhl* deficiency. To further interrogate this working hypothesis, qRT-PCR was performed on NIH 3T3 cells with knockout of *Vhl*, *Pbrm1*, or both using CRISPR-Cas9. Indeed, the loss of PBRM1 further enhances HIF1 and the STAT3 signaling that was primed upon the loss of VHL (Figure S6G).

### The Expression of OXPHOS Genes Is Markedly Downregulated in *Vhl* and *Pbrm1* Doubly Deficient Mouse Kidneys

In contrast to cluster I that encompasses upregulated genes in the *Vhl*<sup>F/F</sup>*Pbrm1*<sup>F/F</sup>*Ksp-Cre* kidneys, cluster III mainly consists of significantly downregulated genes (Figure 5A) within which most enriched are OXPHOS genes (Figure 5B). The significant downregulation of nuclear-encoded OXPHOS genes was further confirmed by qRT-PCR of genes involved in different electron-transport chain complexes, including *Ndufa2* (complex I), *Sdhb* (complex II), *Cox5a* (complex IV), and *Atp4a* (complex V) (Figures 5D, S6E, and S6F). HOMER analysis was performed to determine if specific transcription factors might have directly mediated such repression. However, we did not detect enrichment of any pertinent TFBMs within the cluster III genes. It has been shown that HIF1 inhibits mitochondrial biogenesis and respiration through downregulation of PGC1 $\beta$  transcription in RCC4, a VHL-deficient human kidney cancer cell line (Zhang et al., 2007). However, neither gene expression profiling nor qRT-PCR detected significant downregulation of *Pgc1 $\beta$*  in *Vhl*<sup>F/F</sup>*Pbrm1*<sup>F/F</sup>*Ksp-Cre* kidneys (Figure S6F). TCGA pan-kidney cancer analysis on common human kidney cancer types, including KIRC (kidney renal clear), KIRP (kidney renal papillary), and KICH (kidney chromophobe), demonstrated a significant downregulation of OXPHOS genes in ccRCC, but not in papillary RCC (pRCC) or chromophobe RCC (chRCC) (Chen et al., 2016).

### *Vhl* and *Pbrm1* Doubly Deficient Clear Cell Kidney Tumors Display Hyperactive mTORC1 Signaling

The observation that clear cell kidney tumors occurred in *Vhl*<sup>F/F</sup>*Pbrm1*<sup>F/F</sup>*Ksp-Cre* mice after a long latency period suggests the involvement of additional genetic and/or epigenetic events. To investigate whether transcriptional aberrations might be responsible, RNA sequencing (RNA-seq) was performed on *Vhl*<sup>F/F</sup>*Pbrm1*<sup>F/F</sup>*Ksp-Cre* kidney tumors and age-matched *WT* renal cortices. The complex pathological changes observed in the aged *Vhl*<sup>F/F</sup>*Pbrm1*<sup>F/F</sup>*Ksp-Cre* mouse kidneys precluded the isolation of adjacent normal renal cortices for comparison.

Differentially expressed genes were identified (Table S3) and subjected to unsupervised hierarchical clustering analysis, which identified two clusters denoting tumors and normal

controls (Figure 6A). These genes were analyzed and visualized with ClueGO to interrogate functionally grouped gene ontology and pathway networks (Figure 6B; Table S4). Gene Set Enrichment Analysis (GSEA) revealed upregulation of HIF1 and STAT3 pathways and downregulation of OXPHOS pathway in *Vhl*<sup>F/F</sup>*Pbrm1*<sup>F/F</sup>*Ksp-Cre* tumors (Figure 6C), consistent with the findings observed in the 12-week-old *Vhl*<sup>F/F</sup>*Pbrm1*<sup>F/F</sup>*Ksp-Cre* renal cortices (Figure 5B). Significantly, dysregulation of the mTOR signaling pathway was shown in the *Vhl* and *Pbrm1* doubly deficient tumors but not in the 12-week-old *Vhl*<sup>F/F</sup>*Pbrm1*<sup>F/F</sup>*Ksp-Cre* renal cortices (Figures 5B, 6B, and 6C; Table S4). To validate RNA-sequencing findings, qRT-PCR focused on the HIF1 and mTOR pathway genes was performed (Figures 6E and 6F), which demonstrated consistent findings among gene expression analysis platforms. We also performed immunohistochemistry on *Vhl*<sup>F/F</sup>*Pbrm1*<sup>F/F</sup>*Ksp-Cre* mouse tumors to assess HIF1 and mTOR signaling. A significant nuclear accumulation of HIF1, a weak nuclear accumulation of HIF2, and an expression of GLUT1, an HIF target, were detected in these tumors (Figure S7A). Furthermore, increased phosphorylation of 4E-BP1 and S6K, two well-established mTORC1 substrates, were detected in *Vhl*<sup>F/F</sup>*Pbrm1*<sup>F/F</sup>*Ksp-Cre* tumors but not adjacent normal-looking kidney tissues (Figures 6D and S7B). In contrast, the phosphorylation of ERK was not increased in the *Vhl* and *Pbrm1* doubly deficient kidney tumors (Figure 6D).

It is noteworthy that *Ddit4* or *Redd1*, a transcriptional target of HIF1 (Brugarolas et al., 2004), was significantly upregulated in *Vhl* and *Pbrm1* doubly deficient kidney tumors (Figure 6E). REDD1 is known to suppress mTORC1 activity by releasing TSC2 from its inhibitor 14-3-3 (Brugarolas et al., 2004; DeYoung et al., 2008). Several lines of clinical evidence support the importance of mTORC1 activation in the pathobiology of human ccRCC, including the known therapeutic benefit of administering mTORC1 inhibitors in treating metastatic ccRCC (Voss et al., 2014; Wei and Hsieh, 2015) and the observed prevalent mTORC1 pathway activation in human ccRCC (Linehan et al., 2010; Robb et al., 2007). Induction of REDD1 by HIF1 may activate a tumor suppressor checkpoint that restrains the oncogenic potential of HIF1. Hence, activation of mTORC1 activity through additional genetic/epigenetic events may be required for the initiation of ccRCC in *Vhl* and *Pbrm1* doubly deficient renal epithelial cells. In fact, significant downregulation of *Tsc1* and *Tsc2* was demonstrated in *Vhl* and *Pbrm1* doubly deficient kidney tumors (Figure 6F), which would activate mTORC1 even when REDD1 was upregulated. In summary, the emergent mTORC1 activation detected in the *Vhl* and *Pbrm1* doubly deficient ccRCC may represent a prerequisite oncogenic driver event in the pathogenesis of ccRCC once kidney epithelial cells lost VHL and PBRM1.

### Analyses of Mouse and Human ccRCC Reveal Convergence on the mTOR Pathway Activation

Contrary to the inability of *Vhl* deficiency to initiate ccRCC in mice, the *Hif1 $\alpha$ -M3* transgenic model (*Hif1 $\alpha$ -M3* TRACK) where kidney-specific overexpression of a non-degradable as well as transcriptionally active mutant HIF1 $\alpha$ -M3 (P402A, F564A, N803A) resulted in renal cysts and small clear cell tumors in aged (14–22 months) mice (Fu et al., 2011, 2015). Of note,

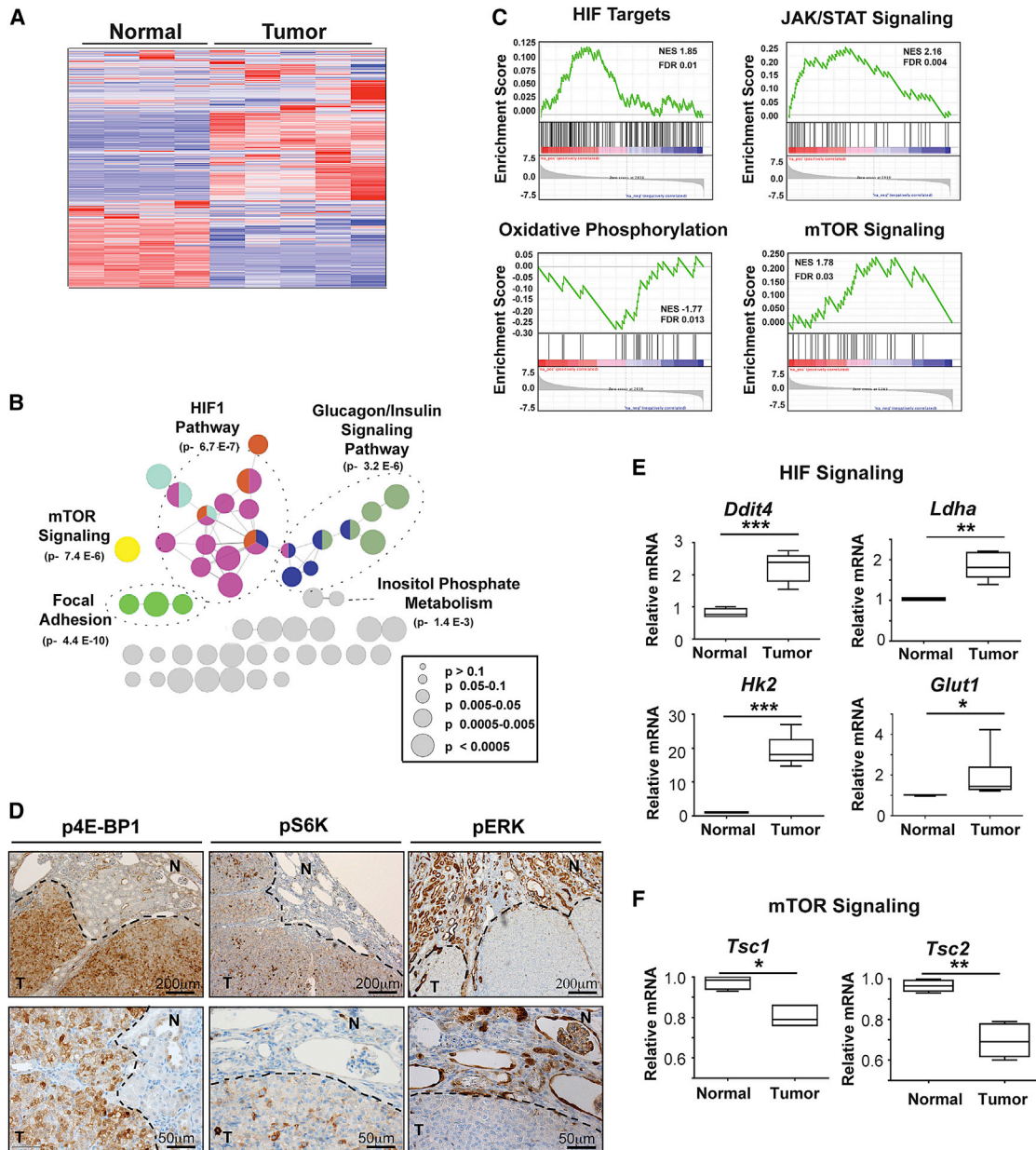


**Figure 6. *Vhl* and *Pbrm1* Doubly Deficient Clear Cell Kidney Tumors Display Hyperactive mTORC1 Signaling**

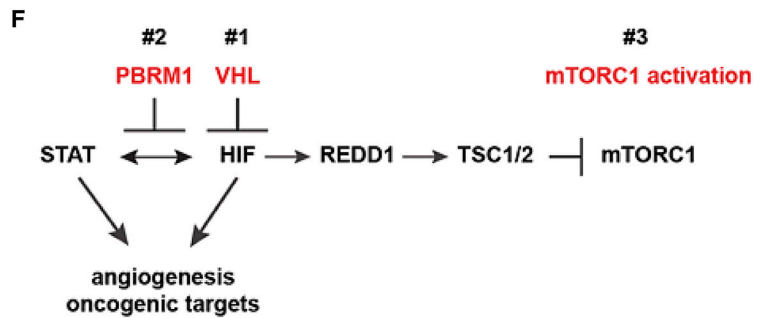
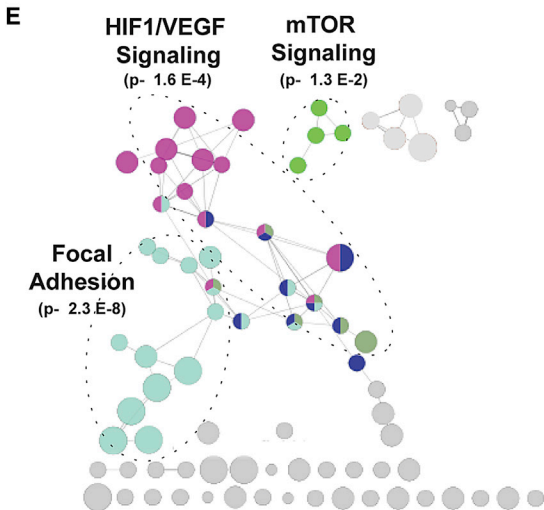
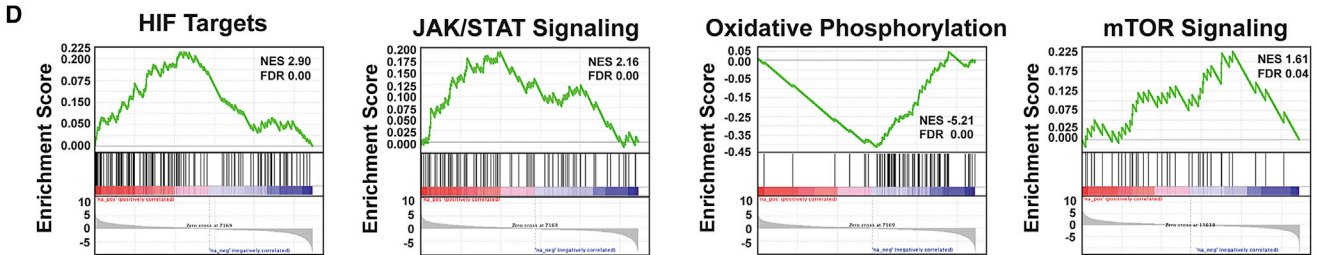
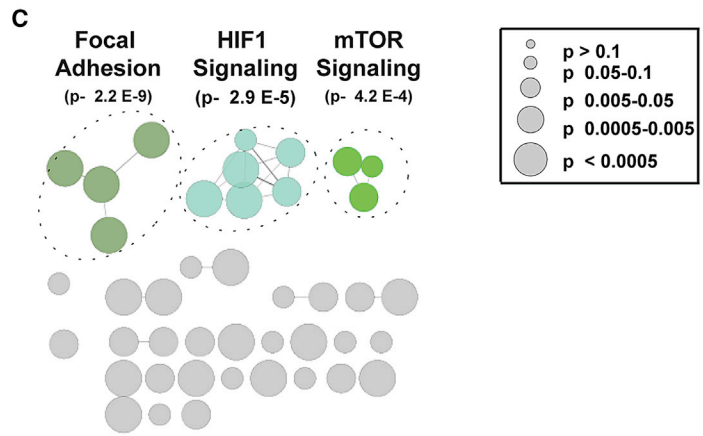
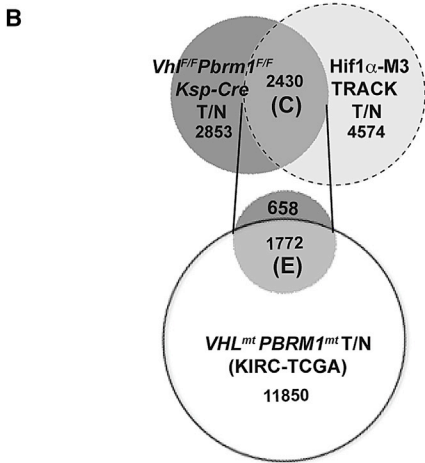
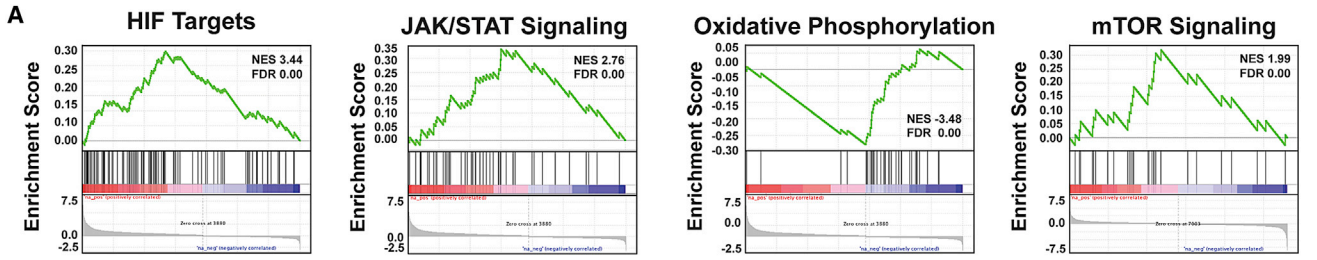
(A) Heatmap of genes with significantly different expression in age-matched WT kidneys (n = 4) and *Vhl*<sup>F/F</sup>*Pbrm1*<sup>F/F</sup>*Ksp-Cre* tumors (n = 5) based on unsupervised hierarchical agglomerative clustering.

(B) The genes that were significantly, differentially expressed in *Vhl*<sup>F/F</sup>*Pbrm1*<sup>F/F</sup>*Ksp-Cre* T/N (false discovery rate [FDR] < 0.05) were tested for enrichment and represented using ClueGO.

(C) GSEA plots of the ranked list of differentially expressed genes in *Vhl*<sup>F/F</sup>*Pbrm1*<sup>F/F</sup>*Ksp-Cre* kidney tumors (T) and WT normal kidneys (N) generated using three gene sets: curated HIF targets, KEGG JAK STAT signaling pathway, KEGG oxidative phosphorylation pathway, and KEGG mTOR Pathway enrichment.

(D) Immunohistochemistry of phosphorylated-4E-BP1 (p4E-BP1) at threonine 37/46 (column 1), phosphorylated S6K (pS6K) at serine 240/244 (column 2), and phosphorylated ERK1/2 (pERK) at threonine 202/tyrosine 204 in *Vhl*<sup>F/F</sup>*Pbrm1*<sup>F/F</sup>*Ksp-Cre* tumors. T, tumor; N, adjacent normal. Scale bars are at 100  $\mu$ m or 200  $\mu$ m as indicated.

(E and F) The mRNA levels of *Ddit4* (E, top left), *Ldha* (E, top right), *Hk2* (E, bottom left), *Glut1* (E, bottom right), *Tsc1* (F, left), and *Tsc2* (F, right) in *Vhl*<sup>F/F</sup>*Pbrm1*<sup>F/F</sup>*Ksp-Cre* tumors (n = 6) and WT kidneys (n = 4) were assessed by qRT-PCR. Data were normalized against GAPDH (mean  $\pm$  SD). \*p < 0.05; \*\*p < 0.005; \*\*\*p < 0.0005 (Student's t test).



(legend on next page)

oxygen-dependent hydroxylation of P402 and F564 of HIF1 $\alpha$  by prolyl hydroxylase domain enzymes (PHDs) and of N803 by factor inhibiting HIF (FIH) enhances the HIF-VHL interaction, leading to its degradation (Keith et al., 2011; Masson and Ratcliffe, 2014). Furthermore, hydroxylation of N803 by FIH also disrupts the interaction between HIF and transcription coactivator p300/CBP, thereby inhibiting HIF1-mediated transcription (Masson and Ratcliffe, 2014). Although VHL loss leads to the stabilization of HIF1 $\alpha$  and HIF2 $\alpha$ , oxygen-dependent and FIH1-mediated asparaginyl hydroxylation of HIFs prevents the recruitment of p300/CBP, which helps explain why *Vhl* deficiency alone is insufficient for kidney tumor initiation.

To further determine whether mTORC1 activation might be a mechanistically preferred node after the hyperactivation of HIF1 during the pathogenesis of ccRCC, we resorted to the transcriptomic data of the *Hif1 $\alpha$ -M3* TRACK mouse model. Indeed, GSEA revealed upregulation of the mTOR signaling pathway (Figure 7A). As expected, upregulation of HIF1 and JAK/STAT signaling pathways and downregulation of the OXPHOS pathway were also seen in the *Hif1 $\alpha$ -M3* TRACK mouse model (Figure 7A). We further compared the transcriptomics of the *Vhl<sup>F/F</sup>Pbrm1<sup>F/F</sup>Ksp-Cre* tumors to those of the *Hif1 $\alpha$ -M3* TRACK mouse model (Figure 7B). Within the 2,430 differentially expressed genes shared between these two models, enrichment in the mTOR and HIF1 pathways was evident (Figures 7B and 7C; Table S5). The shared mTOR pathway aberration between these two different mouse ccRCC models supports the convergence on mTORC1 activation once HIF1 becomes hyperactive (Figures 7A–7C).

To determine whether this observation could be extended into human ccRCC bearing both *VHL* and *PBRM1* mutations, we first compiled differentially expressed genes in human *VHL*- and *PBRM1*-mutated ccRCC from the TCGA-KIRC dataset. Consistent with the findings observed in mouse ccRCC, GSEA of these differentially expressed genes revealed upregulation of HIF1, JAK/STAT3, and mTOR pathways and the downregulation of OXPHOS pathway (Figure 7D). Next, we compared the differentially expressed genes identified in human *VHL*- and *PBRM1*-mutated ccRCC to those shared between the two mouse models, which resulted in the identification of 1,772 genes that were shared among these three ccRCC models (Figure 7B). Within this shared gene set, HIF1 and mTOR pathway genes were statistically enriched again (Figure 7E; Table S6). Taken together, our study favors a scenario in which a sequence of at least three distinct genetic/epigenetic events including the loss of VHL, the loss of PBRM1, and the subsequent activa-

tion of mTORC1 are required for the development of ccRCC (Figure 7F).

## DISCUSSION

*VHL* is the most commonly mutated gene in human ccRCC and its mutation serves as the initial driver event in the pathogenesis of ccRCC (Linehan et al., 1995). However, genetic deletion of *Vhl* in mice is insufficient to initiate kidney tumors (Haase et al., 2001; Kapitsinou and Haase, 2008), favoring the involvement of additional genetic/epigenetic events. Such events remained elusive till the discovery of additional 3p21 tumor suppressor genes commonly mutated in human ccRCC, i.e., *PBRM1*, *SETD2*, and *BAP1* (Hakimi et al., 2013b). Although *PBRM1* is the second most commonly mutated gene in human ccRCC, whether and how *PBRM1* loss contributes to the pathogenesis of ccRCC are unknown. Through tissue-specific deletion of both *Vhl* and *Pbrm1* (*Vhl<sup>F/F</sup>Pbrm1<sup>F/F</sup>Ksp-Cre*), we created a clear cell kidney cancer mouse model that recapitulates histopathological and molecular features of human ccRCC and elucidated how *PBRM1* functions as a tumor suppressor in ccRCC.

The *Vhl<sup>F/F</sup>Pbrm1<sup>F/F</sup>Ksp-Cre* mice developed preneoplastic polycystic kidney lesions at ~6 months and multifocal ccRCC at ~10 months, suggesting that loss of *Vhl* and *Pbrm1* in kidney predisposes to ccRCC. The human pan-cancer genomics identified SWI/SNF complexes as commonly mutated genes (~20%) across cancer types with preferential enrichment of individual mutations in specific cancer types (Helming et al., 2014; Kadoch et al., 2013; Marquez et al., 2015), which presents challenges and opportunities in broadening our knowledge on how chromatin remodeling ATPase complexes function as tumor suppressors. Among the SWI/SNF complexes, SMARCB1 (BAF47) is the best-characterized tumor suppressor that regulates cell cycle and antagonizes PRC2 complex (Helming et al., 2014). Expression profiling of 12-week-old *Vhl<sup>F/F</sup>Pbrm1<sup>F/F</sup>Ksp-Cre* renal cortices revealed the tumor suppressor role of *PBRM1* in preventing the self-perpetuating over-amplification of the HIF1 pathway through limiting the intricate feed-forward interplay between HIF1 and STAT3 upon VHL loss (Demaria and Poli, 2012; Jung et al., 2005; Luo and Semenza, 2012). The unexpected tumor suppressor function of *PBRM1* is analogous to an electrical resistor in preventing power overdrive, in which *PBRM1* restrains the HIF1 and STAT3 transcription outputs from over-amplification upon the loss of VHL (Figure 7F).

The observation that clear cell kidney tumors occurred in *Vhl<sup>F/F</sup>Pbrm1<sup>F/F</sup>Ksp-Cre* mice after a long latency period

### Figure 7. Analyses of Mouse and Human ccRCC Reveal Convergence on the mTOR Pathway Activation

(A) GSEA plots of the ranked list of differentially expressed genes in *Hif1 $\alpha$ -M3* TRACK mouse tumors (T) and normal (N) generated using four gene sets: curated HIF targets, KEGG JAK STAT signaling pathway, KEGG oxidative phosphorylation pathway, and KEGG mTOR Pathway.

(B) Venn diagram of differentially expressed genes in *Vhl<sup>F/F</sup>Pbrm1<sup>F/F</sup>Ksp-Cre* tumors (T) versus WT normal (N) (T/N), *Hif1 $\alpha$ -M3* TRACK T/N samples, and human *VHL<sup>mt</sup>PBRM1<sup>mt</sup>* ccRCC tumors versus normal.

(C) The differentially expressed genes at the intersect of *Vhl<sup>F/F</sup>Pbrm1<sup>F/F</sup>Ksp-Cre* T/N and *Hif1 $\alpha$ -M3* TRACK T/N were tested for enrichment and presented using ClueGO.

(D) GSEA plots of the ranked list of differentially expressed genes in human *VHL<sup>mt</sup>PBRM1<sup>mt</sup>* ccRCC tumors versus normal kidneys generated using four gene sets: curated HIF targets, KEGG JAK STAT signaling pathway, KEGG oxidative phosphorylation pathway, and KEGG mTOR Pathway.

(E) The shared differentially expressed genes in *Vhl<sup>F/F</sup>Pbrm1<sup>F/F</sup>Ksp-Cre* T/N, *Hif1 $\alpha$ -M3* TRACK T/N, and TCGA-KIRC *VHL<sup>mt</sup>PBRM1<sup>mt</sup>* T/N were tested for enrichment and presented using ClueGO.

(F) Model depicts the chronological sequences of genetic and signaling events during the pathogenesis of *Vhl* and *Pbrm1* doubly deficient ccRCC.

suggests the involvement of additional signaling aberrations. Immunohistochemical and transcriptomic analyses demonstrated that activation of mTORC1 rather than the ERK pathway is the preferred third event. Ample evidences support the importance of mTORC1 activation in the pathobiology of human ccRCC, e.g., mTORC1 pathway activation is prevalent in human ccRCC (Linehan et al., 2010; Robb et al., 2007) and mTOR inhibitors are standard of care in treating metastatic ccRCC (Voss et al., 2014; Wei and Hsieh, 2015). As REDD1, a key transcriptional target of HIF1, negatively regulates mTORC1 through activation of TSC1/TSC2 (Brugarolas et al., 2004; DeYoung et al., 2008), it is foreseeable that mTORC1 activation could be a bottleneck for tumors originating from a hyperactive HIF1 signaling. Consistent with this working hypothesis, both the *Vhl<sup>F/F</sup>Pbrm1<sup>F/F</sup>Ksp-Cre* and the published HIF1 $\alpha$ -M3 TRACK mouse models (Fu et al., 2011) developed ccRCC after a long latency period and showed convergence on mTORC1 activation (Figure 7F). Moreover, mTORC1 pathway activation was also observed in human ccRCC carrying mutations of *VHL* and *PBRM1* (Figure 6E). Of note, multi-regional sequencing of a hereditary VHL syndrome patient also detected the mutations of *PBRM1* and the convergence of mTORC1 pathway activation (Fisher et al., 2014). These findings are consistent with a recurrent oncogenic theme in which many oncogenes, such as c-MYC, BRAF, and MLL-fusions, activate both oncogenic signaling and intrinsic tumor-suppressor checkpoints (Liu et al., 2014; Lowe et al., 2004; Maertens et al., 2013). Therefore, abrogating the built-in intrinsic tumor suppressor activities of individual oncogenes is essential for tumorigenesis. It was recently reported that homozygous deletion of *Vhl* and *Bap1* in mouse kidney resulted in early lethality (<1 month), and some mice (within a cohort of 7) carrying homozygous deletion of *Vhl* and heterozygous deletion of *Bap1* developed tumor micronodules (0.25–1.8 mm) with unknown tumor incidence, transplantability, and molecular characteristics (Wang et al., 2014). Notably, complete BAP1 inactivation is observed in human ccRCC (Peña-Llopis et al., 2012). How heterozygous loss of *Bap1* cooperates with *Vhl* loss to initiate kidney tumorigenesis in mice remains intriguing (Wang et al., 2014).

The suppression of OXPHOS genes observed in the *Vhl<sup>F/F</sup>Pbrm1<sup>F/F</sup>Ksp-Cre* ccRCC model is consistent with the global metabolomics reported on ccRCC (Hakimi et al., 2016), which lends further support for the notion that kidney cancer is a metabolic disease that manifests with massive metabolic reprogramming (Hakimi et al., 2016; Linehan et al., 2010). Inhibitors of mTORC1, the key cellular complex integrating nutrient and growth factor signaling to promote anabolic metabolism, are standard of care for metastatic ccRCC (Voss and Hsieh, 2016). However, a wide range of clinical outcomes has been observed. Interestingly, genomic study of RECORD-3, a large clinical trial that randomized kidney cancer patients to either VEGFR or mTORC1 inhibitors, demonstrated that ccRCC with mutant *PBRM1* associates with longer progression free survival (PFS) on everolimus, an mTORC1 inhibitor, at 12.8 months than those with wild-type *PBRM1* at 5.5 months (Hsieh et al., 2015, 2017a). In parallel, the *Vhl<sup>F/F</sup>Pbrm1<sup>F/F</sup>Ksp-Cre* ccRCC and human *VHL*- and *PBRM1*-mutated ccRCC shared mTORC1 pathway aberration. Both clinical data and this study support a

model in which mTORC1 activation constitutes the preferred third driver event during ccRCC tumorigenesis immediately after genetic inactivation of *VHL* and *PBRM1* (Voss and Hsieh, 2016) (Figure 7F), which serves as an example of preferential pathway convergent evolution of a given cancer type (Voss and Hsieh, 2016; Wei and Hsieh, 2015) that could have predictive values for selecting patients of a given cancer genotype with matched targeted therapies.

## EXPERIMENTAL PROCEDURES

More detailed information is available in the Supplemental Experimental Procedures.

### Mice

*Baf180<sup>F/F</sup>* mice were obtained from Dr. Wang Zhong (Wurster et al., 2012). Animal experiments were performed in accordance to the Institutional Animal Care and Use Committee (IACUC) at MSKCC.

### Mouse MRI

Mice MRI scans were carried out on either 200 or 300 MHz Bruker 4.7 T or 7 T Biospec scanners (Bruker Biospin MRI GmbH) equipped with 640 mT/m ID 115 mm and 300 mT/m ID 200 mm gradients, respectively (Resonance Research).

### RNA Isolation and Microarray Analysis

Total RNA was isolated using TRIzol (Life Technologies) and cleaned up using QIAGEN column DNase digestion. RNA samples were prepared from 3-month-old *Ksp-Cre*, *Vhl<sup>F/F</sup>Ksp-Cre*, *Pbrm1<sup>F/F</sup>Ksp-Cre*, and *Vhl<sup>F/F</sup>Pbrm1<sup>F/F</sup>Ksp-Cre* mice. Microarray was performed by Integrated Genomics Operation (IGO) at MSKCC.

### RNA-Seq and Analysis

Total RNA was processed by the IGO using TruSeq RNA Sample Prep kit according to the manufacturer's recommendation. Gene ontology (GO) analysis of mouse microarray and RNA-seq data were performed with ClueGO.

### Motif Activity Analysis

To analyze activities of transcription factor binding motifs (TFBM) using RNA-seq data, we used the Integrated System for Motif Activity Response Analysis (ISMARA).

### ACCESSION NUMBERS

The accession numbers for the RNA-seq and affy array data reported in this paper are GEO: GSE83688 and GSE83597, respectively.

### SUPPLEMENTAL INFORMATION

Supplemental Information includes Supplemental Experimental Procedures, seven figures, and seven tables and can be found with this article online at <http://dx.doi.org/10.1016/j.celrep.2017.02.074>.

### AUTHOR CONTRIBUTIONS

M.B. and Z.D. initiated the study. A.M.N., C.G.P., and Y.D. designed and conducted experiments and analyzed data. A.M.N. is responsible for molecular, C.G.P. for phenotypic, and Y.D. for allograft studies. Y.X., T.O., S.T., S.H., and C.E.R. conducted some experiments. P.I.W., H.U.O., and C.J.C. analyzed data. C.L.L. and J.A.K. performed MRI. O.A. evaluated MRI. S.M. and S.K.T. performed histopathological examination. C.S.L., N.W., A.A.H., and W.L. supervised data analyses. Z.W. provided the *PBRM1* conditional knockout mice. J.J.H. conceived and directed the research study. E.H.C. designed research and supervised the project. J.J.H. and E.H.C. wrote the manuscript.

## ACKNOWLEDGMENTS

This work was supported by The Jill and Jeffrey Weiss Fund to the Cure of Kidney Cancer and J. Randall and Kathleen L. MacDonald Kidney Cancer Research Fund. We thank Dr. Mihaela Lupu, Mr. Dov Winkleman, and Ms. Smrutiben A. Mehta for their technical support, and Dr. Victor Reuter for the initial assessment of mouse renal tumors. The MRI and LCP cores were supported by NIH grant P30CA008748.

Received: January 1, 2016

Revised: January 23, 2017

Accepted: February 24, 2017

Published: March 21, 2017

## REFERENCES

- Adam, J., Hatipoglu, E., O'Flaherty, L., Ternette, N., Sahgal, N., Lockstone, H., Baban, D., Nye, E., Stamp, G.W., Wolhuter, K., et al. (2011). Renal cyst formation in Fh1-deficient mice is independent of the Hif/Phd pathway: roles for fumarate in KEAP1 succination and Nrf2 signaling. *Cancer Cell* 20, 524–537.
- Baba, M., Furihata, M., Hong, S.B., Tessarollo, L., Haines, D.C., Southon, E., Patel, V., Igarashi, P., Alvord, W.G., Leighty, R., et al. (2008). Kidney-targeted Birt-Hogg-Dube gene inactivation in a mouse model: Erk1/2 and Akt-mTOR activation, cell hyperproliferation, and polycystic kidneys. *J. Natl. Cancer Inst.* 100, 140–154.
- Balwierz, P.J., Pachkov, M., Arnold, P., Gruber, A.J., Zavolan, M., and van Nimwegen, E. (2014). ISMARA: automated modeling of genomic signals as a democracy of regulatory motifs. *Genome Res.* 24, 869–884.
- Biegel, J.A., Busse, T.M., and Weissman, B.E. (2014). SWI/SNF chromatin remodeling complexes and cancer. *Am. J. Med. Genet. C. Semin. Med. Genet.* 166C, 350–366.
- Bindea, G., Mlecnik, B., Hackl, H., Charoentong, P., Tosolini, M., Kirilovsky, A., Fridman, W.H., Pagès, F., Trajanoski, Z., and Galon, J. (2009). ClueGO: a Cytoscape plug-in to decipher functionally grouped gene ontology and pathway annotation networks. *Bioinformatics* 25, 1091–1093.
- Brugarolas, J., Lei, K., Hurley, R.L., Manning, B.D., Reiling, J.H., Hafen, E., Witters, L.A., Ellisen, L.W., and Kaelin, W.G., Jr. (2004). Regulation of mTOR function in response to hypoxia by REDD1 and the TSC1/TSC2 tumor suppressor complex. *Genes Dev.* 18, 2893–2904.
- Burrows, A.E., Smogorzewska, A., and Elledge, S.J. (2010). Polybromo-associated BRG1-associated factor components BRD7 and BAF180 are critical regulators of p53 required for induction of replicative senescence. *Proc. Natl. Acad. Sci. USA* 107, 14280–14285.
- Cancer Genome Atlas Research Network (2013). Comprehensive molecular characterization of clear cell renal cell carcinoma. *Nature* 499, 43–49.
- Chen, J., Futami, K., Petillo, D., Peng, J., Wang, P., Knol, J., Li, Y., Khoo, S.K., Huang, D., Qian, C.N., et al. (2008). Deficiency of FLCN in mouse kidney led to development of polycystic kidneys and renal neoplasia. *PLoS ONE* 3, e3581.
- Chen, F., Zhang, Y., Şenbabaoğlu, Y., Ciriello, G., Yang, L., Reznik, E., Shuch, B., Micevic, G., De Velasco, G., Shinbrot, E., et al. (2016). Multilevel genomics-based taxonomy of renal cell carcinoma. *Cell Rep.* 14, 2476–2489.
- Clapier, C.R., and Cairns, B.R. (2009). The biology of chromatin remodeling complexes. *Annu. Rev. Biochem.* 78, 273–304.
- Dawson, M.A., and Kouzarides, T. (2012). Cancer epigenetics: from mechanism to therapy. *Cell* 150, 12–27.
- Demaria, M., and Poli, V. (2012). PKM2, STAT3 and HIF-1 $\alpha$ : The Warburg's vicious circle. *JAK-STAT* 1, 194–196.
- DeYoung, M.P., Horak, P., Sofer, A., Sgroi, D., and Ellisen, L.W. (2008). Hypoxia regulates TSC1/2-mTOR signaling and tumor suppression through REDD1-mediated 14-3-3 shuttling. *Genes Dev.* 22, 239–251.
- Fisher, R., Horswell, S., Rowan, A., Salm, M.P., de Bruin, E.C., Gulati, S., McGranahan, N., Stares, M., Gerlinger, M., Varela, I., et al. (2014). Development of synchronous VHL syndrome tumors reveals contingencies and constraints to tumor evolution. *Genome Biol.* 15, 433.
- Fitzmaurice, C., Dicker, D., Pain, A., Hamavid, H., Moradi-Lakeh, M., MacIntyre, M.F., Allen, C., Hansen, G., Woodbrook, R., Wolfe, C., et al.; Global Burden of Disease Cancer Collaboration (2015). The Global Burden of Cancer 2013. *JAMA Oncol.* 1, 505–527.
- Frew, I.J., Thoma, C.R., Georgiev, S., Minola, A., Hitz, M., Montani, M., Moch, H., and Krek, W. (2008). pVHL and PTEN tumour suppressor proteins cooperatively suppress kidney cyst formation. *EMBO J.* 27, 1747–1757.
- Fu, L., Wang, G., Shevchuk, M.M., Nanus, D.M., and Gudas, L.J. (2011). Generation of a mouse model of Von Hippel-Lindau kidney disease leading to renal cancers by expression of a constitutively active mutant of HIF1 $\alpha$ . *Cancer Res.* 71, 6848–6856.
- Fu, L., Minton, D.R., Zhang, T., Nanus, D.M., and Gudas, L.J. (2015). Genome-wide profiling of TRACK kidneys shows similarity to the human ccRCC transcriptome. *Mol. Cancer Res.* 13, 870–878.
- Gnarra, J.R., Tory, K., Weng, Y., Schmidt, L., Wei, M.H., Li, H., Latif, F., Liu, S., Chen, F., Duh, F.M., et al. (1994). Mutations of the VHL tumour suppressor gene in renal carcinoma. *Nat. Genet.* 7, 85–90.
- Haase, V.H., Glickman, J.N., Socolovsky, M., and Jaenisch, R. (2001). Vascular tumors in livers with targeted inactivation of the von Hippel-Lindau tumor suppressor. *Proc. Natl. Acad. Sci. USA* 98, 1583–1588.
- Hakimi, A.A., Chen, Y.B., Wren, J., Gonen, M., Abdel-Wahab, O., Heguy, A., Liu, H., Takeda, S., Tickoo, S.K., Reuter, V.E., et al. (2013a). Clinical and pathologic impact of select chromatin-modulating tumor suppressors in clear cell renal cell carcinoma. *Eur. Urol.* 63, 848–854.
- Hakimi, A.A., Pham, C.G., and Hsieh, J.J. (2013b). A clear picture of renal cell carcinoma. *Nat. Genet.* 45, 849–850.
- Hakimi, A.A., Reznik, E., Lee, C.H., Creighton, C.J., Brannon, A.R., Luna, A., Aksoy, B.A., Liu, E.M., Shen, R., Lee, W., et al. (2016). An integrated metabolic atlas of clear cell renal cell carcinoma. *Cancer Cell* 29, 104–116.
- Hargreaves, D.C., and Crabtree, G.R. (2011). ATP-dependent chromatin remodeling: genetics, genomics and mechanisms. *Cell Res.* 21, 396–420.
- Helming, K.C., Wang, X., and Roberts, C.W. (2014). Vulnerabilities of mutant SWI/SNF complexes in cancer. *Cancer Cell* 26, 309–317.
- Hsieh, J.J., Chen, D.P.W., Chen, Y.B., Redzematovic, A., and Marker, M. (2015). Identification of efficacy biomarkers in a large metastatic renal cell carcinoma (mRCC) cohort through next generation sequencing (NGS): results from RECORD-3. *J. Clin. Oncol.* 33, abstr 4509.
- Hsieh, J.J., Chen, D., Wang, P.I., Marker, M., Redzematovic, A., Chen, Y.B., Selcuklu, S.D., Weinhold, N., Bouvier, N., Huberman, K.H., et al. (2017a). Genomic biomarkers of a randomized trial comparing first-line everolimus and sunitinib in patients with metastatic renal cell carcinoma. *Eur. Urol.* 71, 405–414.
- Hsieh, J.J., Purdue, M.P., Signoretti, S., Swanton, C., Albiges, L., Schmidinger, M., Heng, D.Y., Larkin, J., and Ficarra, V. (2017b). Renal cell carcinoma. *Nat. Rev. Dis. Primers* 3, 17009.
- Huang, X., Gao, X., Diaz-Trelles, R., Ruiz-Lozano, P., and Wang, Z. (2008). Coronary development is regulated by ATP-dependent SWI/SNF chromatin remodeling component BAF180. *Dev. Biol.* 319, 258–266.
- Igarashi, P. (2004). Kidney-specific gene targeting. *J. Am. Soc. Nephrol.* 15, 2237–2239.
- Jung, J.E., Lee, H.G., Cho, I.H., Chung, D.H., Yoon, S.H., Yang, Y.M., Lee, J.W., Choi, S., Park, J.W., Ye, S.K., and Chung, M.H. (2005). STAT3 is a potential modulator of HIF-1-mediated VEGF expression in human renal carcinoma cells. *FASEB J.* 19, 1296–1298.
- Kadoch, C., Hargreaves, D.C., Hodges, C., Elias, L., Ho, L., Ranish, J., and Crabtree, G.R. (2013). Proteomic and bioinformatic analysis of mammalian SWI/SNF complexes identifies extensive roles in human malignancy. *Nat. Genet.* 45, 592–601.
- Kaelin, W.G. (2007). Von Hippel-Lindau disease. *Annu. Rev. Pathol.* 2, 145–173.
- Kapitsinou, P.P., and Haase, V.H. (2008). The VHL tumor suppressor and HIF: insights from genetic studies in mice. *Cell Death Differ.* 15, 650–659.

- Keith, B., Johnson, R.S., and Simon, M.C. (2011). HIF1 $\alpha$  and HIF2 $\alpha$ : sibling rivalry in hypoxic tumour growth and progression. *Nat. Rev. Cancer* 12, 9–22.
- Linehan, W.M., Lerman, M.I., and Zbar, B. (1995). Identification of the von Hippel-Lindau (VHL) gene. Its role in renal cancer. *JAMA* 273, 564–570.
- Linehan, W.M., Srinivasan, R., and Schmidt, L.S. (2010). The genetic basis of kidney cancer: a metabolic disease. *Nat. Rev. Urol.* 7, 277–285.
- Liu, H., Westergard, T.D., Cashen, A., Piwnica-Worms, D.R., Kunkle, L., Vij, R., Pham, C.G., DiPersio, J., Cheng, E.H., and Hsieh, J.J. (2014). Proteasome inhibitors evoke latent tumor suppression programs in pro-B MLL leukemias through MLL-AF4. *Cancer Cell* 25, 530–542.
- Lowe, S.W., Cepero, E., and Evan, G. (2004). Intrinsic tumour suppression. *Nature* 432, 307–315.
- Luo, W., and Semenza, G.L. (2012). Emerging roles of PKM2 in cell metabolism and cancer progression. *Trends Endocrinol. Metab.* 23, 560–566.
- Maertens, O., Johnson, B., Hollstein, P., Frederick, D.T., Cooper, Z.A., Messiaen, L., Bronson, R.T., McMahon, M., Granter, S., Flaherty, K., et al. (2013). Elucidating distinct roles for NF1 in melanomagenesis. *Cancer Discov.* 3, 338–349.
- Majmundar, A.J., Wong, W.J., and Simon, M.C. (2010). Hypoxia-inducible factors and the response to hypoxic stress. *Mol. Cell* 40, 294–309.
- Mandriota, S.J., Turner, K.J., Davies, D.R., Murray, P.G., Morgan, N.V., Souter, H.M., Wykoff, C.C., Maher, E.R., Harris, A.L., Ratcliffe, P.J., and Maxwell, P.H. (2002). HIF activation identifies early lesions in VHL kidneys: evidence for site-specific tumor suppressor function in the nephron. *Cancer Cell* 1, 459–468.
- Marquez, S.B., Thompson, K.W., Lu, L., and Reisman, D. (2015). Beyond mutations: additional mechanisms and implications of SWI/SNF complex inactivation. *Front. Oncol.* 4, 372.
- Masson, N., and Ratcliffe, P.J. (2014). Hypoxia signaling pathways in cancer metabolism: the importance of co-selecting interconnected physiological pathways. *Cancer Metab.* 2, 3.
- Neumann, H.P., and Zbar, B. (1997). Renal cysts, renal cancer and von Hippel-Lindau disease. *Kidney Int.* 51, 16–26.
- Peña-Llopis, S., Vega-Rubin-de-Celis, S., Liao, A., Leng, N., Pavia-Jiménez, A., Wang, S., Yamasaki, T., Zhrebker, L., Sivanand, S., Spence, P., et al. (2012). BAP1 loss defines a new class of renal cell carcinoma. *Nat. Genet.* 44, 751–759.
- Rini, B.I., Campbell, S.C., and Escudier, B. (2009). Renal cell carcinoma. *Lancet* 373, 1119–1132.
- Robb, V.A., Karbowniczek, M., Klein-Szanto, A.J., and Henske, E.P. (2007). Activation of the mTOR signaling pathway in renal clear cell carcinoma. *J. Urol.* 177, 346–352.
- Sato, Y., Yoshizato, T., Shiraishi, Y., Maekawa, S., Okuno, Y., Kamura, T., Shimamura, T., Sato-Otsubo, A., Nagae, G., Suzuki, H., et al. (2013). Integrated molecular analysis of clear-cell renal cell carcinoma. *Nat. Genet.* 45, 860–867.
- Semenza, G.L. (2013). HIF-1 mediates metabolic responses to intratumoral hypoxia and oncogenic mutations. *J. Clin. Invest.* 123, 3664–3671.
- Shao, X., Somlo, S., and Igarashi, P. (2002). Epithelial-specific Cre/lox recombination in the developing kidney and genitourinary tract. *J. Am. Soc. Nephrol.* 13, 1837–1846.
- Siegel, R.L., Miller, K.D., and Jemal, A. (2016). Cancer statistics, 2016. *CA Cancer J. Clin.* 66, 7–30.
- Varela, I., Tarpey, P., Raine, K., Huang, D., Ong, C.K., Stephens, P., Davies, H., Jones, D., Lin, M.L., Teague, J., et al. (2011). Exome sequencing identifies frequent mutation of the SWI/SNF complex gene PBRM1 in renal carcinoma. *Nature* 469, 539–542.
- Voss, M.H., and Hsieh, J.J. (2016). Therapeutic guide for mTOuRing through the Braided Kidney Cancer Genomic River. *Clin. Cancer Res.* 22, 2320–2322.
- Voss, M.H., Hsieh, J.J., and Motzer, R.J. (2013). Novel approaches targeting the vascular endothelial growth factor axis in renal cell carcinoma. *Cancer J.* 19, 299–306.
- Voss, M.H., Hakimi, A.A., Pham, C.G., Brannon, A.R., Chen, Y.B., Cunha, L.F., Akin, O., Liu, H., Takeda, S., Scott, S.N., et al. (2014). Tumor genetic analyses of patients with metastatic renal cell carcinoma and extended benefit from mTOR inhibitor therapy. *Clin. Cancer Res.* 20, 1955–1964.
- Walther, M.M., Lubensky, I.A., Venzon, D., Zbar, B., and Linehan, W.M. (1995). Prevalence of microscopic lesions in grossly normal renal parenchyma from patients with von Hippel-Lindau disease, sporadic renal cell carcinoma and no renal disease: clinical implications. *J. Urol.* 154, 2010–2015.
- Wang, Z., Zhai, W., Richardson, J.A., Olson, E.N., Meneses, J.J., Firpo, M.T., Kang, C., Skarnes, W.C., and Tjian, R. (2004). Polybromo protein BAF180 functions in mammalian cardiac chamber maturation. *Genes Dev.* 18, 3106–3116.
- Wang, S.S., Gu, Y.F., Wolff, N., Stefanius, K., Christie, A., Dey, A., Hammer, R.E., Xie, X.J., Rakheja, D., Pedrosa, I., et al. (2014). Bap1 is essential for kidney function and cooperates with Vhl in renal tumorigenesis. *Proc. Natl. Acad. Sci. USA* 111, 16538–16543.
- Wei, E.Y., and Hsieh, J.J. (2015). A river model to map convergent cancer evolution and guide therapy in RCC. *Nat. Rev. Urol.* 12, 706–712.
- Wurster, A.L., Precht, P., Becker, K.G., Wood, W.H., 3rd, Zhang, Y., Wang, Z., and Pazin, M.J. (2012). IL-10 transcription is negatively regulated by BAF180, a component of the SWI/SNF chromatin remodeling enzyme. *BMC Immunol.* 13, 9.
- Xia, W., Nagase, S., Montia, A.G., Kalachikov, S.M., Keniry, M., Su, T., Memeo, L., Hibshoosh, H., and Parsons, R. (2008). BAF180 is a critical regulator of p21 induction and a tumor suppressor mutated in breast cancer. *Cancer Res.* 68, 1667–1674.
- Zhang, H., Gao, P., Fukuda, R., Kumar, G., Krishnamachary, B., Zeller, K.I., Dang, C.V., and Semenza, G.L. (2007). HIF-1 inhibits mitochondrial biogenesis and cellular respiration in VHL-deficient renal cell carcinoma by repression of C-MYC activity. *Cancer Cell* 11, 407–420.